

Investigation the Robustness of Standard Classification Methods for Defining Urban Heat Islands

Yingshuang Lu, Tong He, Xinliang Xu, and Zhi Qiao[✉]

Abstract—In the process of studying the spatiotemporal cause mechanism of urban heat island (UHI) effects, the classification method used will directly affect the robustness of urban surface heat classification. Applying five commonly used standard classification methods, we divided Beijing’s urban surface temperatures in the summer of 2020 into five levels. We then compared the reliability of the five classification methods in resolving 12-period data and the seasonal average temperature in UHI patches, based on two indicators: UHI area and UHI intensity. The actual land-use composition of the UHI patches obtained with traditional methods was applied to confirm our results. The mean-standard deviation method and natural breaks (Jenks) method were more robust with regard to UHI classification and 12-period data reliability. For the UHI area index, the mean-standard deviation method produced the smallest total area of UHI patches for summer days and nights. For the UHI intensity index, the quantile method, mean-standard deviation method, and natural breaks (Jenks) method were associated with smaller errors. Considering the composition of land-use types in UHI patches, the mean-standard deviation method, and natural breaks (Jenks) method were more rigorous. Thus, our research results provide guidance for method selection when classifying UHI.

Index Terms—Moderate resolution imaging spectroradiometer (MODIS) land surface temperature (LST), robustness, standard classification method, urban heat island (UHI) effect, urban thermal grades.

I. INTRODUCTION

UNDER the macrobackground of global climate change, the scope and extent of the impacts of urban climate effects are increasing. An urban heat island (UHI), as the most typical urban climate effect, comprises the accumulation of heat caused by urban buildings and human activity in the urban spaces,

Manuscript received September 6, 2021; revised October 18, 2021; accepted October 25, 2021. Date of publication November 2, 2021; date of current version November 18, 2021. This work was supported in part by the National Natural Science Foundation of China under Grant 41501472 and Grant 41771178, in part by the Scientific and Technological Major Project of Tianjin, China under Grant 18ZXSZSF00240, and in part by the Major Projects of High-Resolution Earth Observation Systems of National Science and Technology under Grant 05-Y30B01-9001-19/20-4. (*Corresponding author:* Zhi Qiao.)

Yingshuang Lu, Tong He, and Zhi Qiao are with the School of Environmental Science and Engineering, Tianjin University, Tianjin 300072, China (e-mail: luyingshuang@tju.edu.cn; hetong160632@163.com; qiaozhi@tju.edu.cn).

Xinliang Xu is with the Institute of Geographical Sciences and Natural Resources Research, Chinese Academy of Sciences State Key Laboratory of Resources and Environmental Information Systems, Beijing 100101, China (e-mail: xuxl@lreis.ac.cn).

Digital Object Identifier 10.1109/JSTARS.2021.3124558

which ultimately leads to a significant temperature difference compared with the suburbs [1]–[6]. The UHI effect affects the regional climate as well as reduces biodiversity and the air and water quality. Moreover, UHI environments promote human disease and increase mortality [7]–[11]. Thus, an effective definition of the spatial scope of the UHI effect is a prerequisite for studying and solving urban thermal environmental problems [12].

In the process of spatial identification of UHI, the classification of land surface thermal power directly affects the accuracy of UHI patch definition [13]–[15]. Thus, finding a stable and reliable classification method is a scientific problem that requires immediate attention. In the current research, a variety of methods were used to classify the UHI patches. For example, Qiao *et al.* applied the mean-standard deviation method to divide the land surface heat field by using the land surface temperature (LST) mean value and 0.5 times the standard deviation to define UHI patches [16], [17]. Fan *et al.* employed the equal interval method to reclassify the normalized LST into different UHI levels [18]. Lin *et al.* and Pan applied the natural break method to spatially classify LST to explore the characteristics of, and mechanism driving spatiotemporal changes in UHIs [19], [20]. Yang *et al.* utilized the defined interval method to classify cities based on the intensity of UHI then applied their findings to classify UHIs [21]. Notably, Smith compared different classification methods from the perspective of spatial mapping: he determined that the quantile method and the mean-standard deviation method were the most effective for datasets with normal distributions [22]. However, to date, few studies have addressed the accuracies of specific classification methods for defining UHI patches or the parameters involved in identifying the optimal technique. It is important to use the most appropriate classification method; this can be achieved by comparing the robustness of individual UHI classification methods and elucidating the reasons for spatial heterogeneity among UHI patches.

In this article, five commonly used standard classification methods—the mean-standard deviation method, equal interval method, natural breaks (Jenks) method, quantile method, and geometric interval method—were used to identify UHI patches and classify the day and night urban LSTs of Beijing, using 12-period data for summer and seasonal average temperatures. Two indicators, the UHI area and UHI intensity, were applied in a comparative analysis of the robustness of the five methods used to classify UHI patches. The actual land use types in each

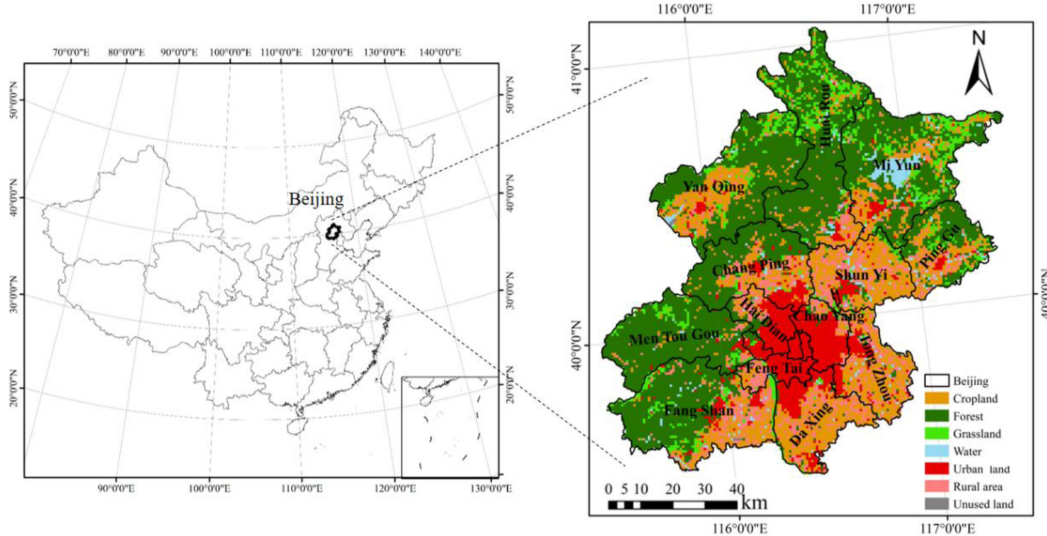


Fig. 1. Geographical location of the study area and land use in this area.

UHI patch were analyzed to verify the robustness of the five classification methods. The kappa coefficient was applied to test the regional consistency of UHI classification as determined by the background field and the five classification methods. The mean-standard deviation method and natural breaks (Jenks) method were more accurate than the other classification methods in defining UHIs. Thus, our results would provide information on the most appropriate classification method for identifying UHIs and the relevant parameters associated with determining the optimal classification strategy.

II. MATERIALS AND METHODS

A. Study Area and Data

Beijing is located in North China and covers an area of 16410.54 km². The summer is hot and rainy, and the winter is cold and dry. It has a typical northern temperate continental monsoon climate. As the political, economic, and cultural center of China, rapidly expanding urban construction in Beijing has encroached on woodland, grassland, and water areas, resulting in an increasingly impacted urban ecological environment, especially, the development of a prominent urban thermal environment that affects the well-being and health of the city's inhabitants (see Fig. 1).

This article was mainly based on LST data, land use data, and altitude (digital elevation model) spatial distribution data. LST data were obtained from the moderate resolution imaging spectroradiometer (MODIS) eight-day average surface temperature product (MOD11A2) for the summer of 2020 (May–July).¹ The transit times of the Terra satellite are 10:30 and 22:30 local solar time. Land use data were acquired from remote-sensing monitoring of land use in China in 2020 and provided by the Resource and Environmental Science and Data Center of the Chinese Academy of Sciences. In the dataset, the various land uses were divided into 6 primary types and 25 secondary types

including cropland, forest, grassland, water area, residential land, unused land [23]. Altitude data were obtained from the Shuttle Radar Topography Mission (SRTM) of the United States Space Shuttle Endeavour. SRTM data are publicly available and have been used on many research platforms to carry out environmental analyses. The spatial resolution of the LST data, land use data, and elevation data used in this article was 1 km.

B. Methods

1) Data Preprocessing: First, we used MODIS reprojection tool data-processing software to preprocess MODIS data (reprojection, data masking, format conversion, etc.) [24]. Quality control (QC) of the preprocessed data was carried out using a QC file to remove cloud-affected pixels in the LST data. Each pixel digital number (DN) was converted to LST, T (unit: °C), as follows:

$$T = DN \times 0.02 - 273.15. \quad (1)$$

To characterize the spatial distribution characteristics of LST in different periods, the preprocessed LST data were normalized, as given [25]:

$$T_n = \frac{T_s - T_{\min}}{T_{\max} - T_{\min}} \quad (2)$$

Where T_n is the normalized value of the LST of a certain pixel. T_s is the actual LST value of the pixel and T_{\max} and T_{\min} are the maximum and minimum LSTs of the area at a certain time, respectively.

2) Comparison of Standard Classification Methods: We selected five common standard classification methods in ArcGIS software platform for the thermal classification of normalized LST data: the mean-standard deviation method; equal interval method; natural breaks (Jenks) method; quantile method; and geometric interval method [26]–[29].

The mean-standard deviation method is defined by the distance each class deviates from the average of all elements. A combination of different standard deviation multiples of the

¹[Online]. Available: <https://ladsweb.modaps.eosdis.nasa.gov/search/>

mean value of the LST was used to divide the land surface heat field, to define a UHI. The method reflects the degree of deviation of the LST from the average temperature in the study area and characterize the temperature variation due to different ground features. However, the outliers in this method tend to distort the average value; thus, most the elements tend to be classified into the same category. We used a 1/2 standard deviation as the classification interval to form the thresholds of different land surface heat levels with respect to the average in the article.

The principle of the equal interval method is to subtract the highest value and the lowest values in the dataset, and then divide the rest of the data into several classes. The advantage of this approach is that the ranges of individual categories are equal, thus simplifying the analysis and explanations. However, if the values have a clustered distribution, rather than a uniform distribution, the first or second category may end up containing more elements, whereas some of the categories may have fewer elements or no elements at all.

The natural breaks (Jenks) method reveals grouping and pattern characteristics inherent in the data. Values within a category are basically similar, whereas values between categories have obvious differences. Thus, data within a cluster are classified into the same category, and separation points are set as gaps between data groups. This method is effectively for grouping similar values and maximizing the difference between classes. Additionally, the technique can accommodate unevenly distributed data values, by self-categorizing clustered data into the same category. However, because the scope of the classes is set separately for each certain dataset, it is difficult to compare outcomes and analyze data across different maps.

Each category in the quantile method contains the same number of elements. This method can draw data with uneven distributions and is capable of determining the relative position of each element. However, elements with the same value may be classified into different categories. In the case of data aggregation, using this method tend to exaggerate the differences between elements. In the case of scattered data, data with large numerical differences may be classified into the same category.

The geometric interval method ensures that the range of each class is approximately the same as the number of values each class has, and the increase from one interval to the next occurs in a very consistent manner. This algorithm is specifically used to process continuous data. This represents a compromise between the equal interval, natural breaks (Jenks), and quantile methods. It strikes a balance between highlighting changes in the intermediate values and taking extreme values into account, such that detailed maps with a smooth appearance are generated.

3) Analyzing the Robustness of Different UHI Classification Methods: After preprocessing 8-day MODIS LST data for Beijing for the summer of 2020, we used the five methods described above to classify 12-period summer data and seasonal day and night average LSTs into temperature grades defining the following five heat zones, ordered from low to high temperatures: the low-temperature zone; the sublow-temperature zone; the medium-temperature zone; the subhigh-temperature zone; and the high-temperature zone. Among them, the subhigh and high temperature zones were defined as UHI patches [30], [31]. The

two UHI indicators, UHI areal percentage and UHII intensity, were then used to explore the robustness of the five classification methods with respect to defining UHI patches.

The calculation methods of UHI area percentage and UHI intensity are as follows:

$$M = \frac{\sum_{i=1}^n A_i}{S} \quad (3)$$

$$P = T_H - T_V \quad (4)$$

where M is the UHI area, i represents the temperature grades with which a UHI is defined, A_i is the area with temperature grade i , S is the area of the study area. P is the UHI intensity. T_H is the average LST of the UHI area, and T_V is the average LST corresponding to that for the middle temperature zone.

III. RESULTS

A. Spatial Pattern of Summer LSTs

ArcGIS software was used to determine the average value of the LST in each of the 12 periods (i.e., summer average values), and the five methods were applied to analyze the data (see Fig. 2). Significant differences were observed among the different classification methods with respect to the spatial distribution and area attributed to each temperature grade.

In terms of spatial distribution, high-temperature and subhigh-temperature areas were distributed in the plain area southeast of Beijing. The distribution during the day was more scattered than that at night. Low-temperature areas were mainly located in the northwest mountainous areas of Beijing.

The spatial distribution of the medium-temperature and sublow-temperature areas differed considerably: during summer days; sublow-temperature; and low-temperature areas, according to the equal interval methods, were distributed in the northeast, north, northwest, and southwest of Beijing. Based on the other classification methods, sublow-temperature and low-temperature areas were scattered throughout these regions. For summer nights, the aggregation of sublow-temperature and low-temperature areas under different classification methods was more obvious than that based on daytime temperatures. Sub-low-temperature and low-temperature areas, as classified using the mean-standard deviation, natural breaks, and quantile methods, were mainly distributed in northeast Beijing and area surrounding the central city. According to the equal interval and geometric interval methods, sub-low-temperature and low-temperature areas were mainly in the north, northwest, and southeast. From the perspective of number of pixels in each image, i.e., (see Fig. 3), the area composition rule, the areas in Beijing in summer (day and night) with high temperatures (level 5), sub-high temperatures (level 4), medium temperatures (level 3), sub-low temperatures (level 2), and low temperatures (level 1) were largely similar. Nevertheless, some differences were observed. Based on the mean-standard deviation and natural breaks methods, the summertime day and night UHI patches, i.e., areas with high and subhigh temperatures, accounted for 27.18–33.39% and 29.57–36.33% of the Beijing

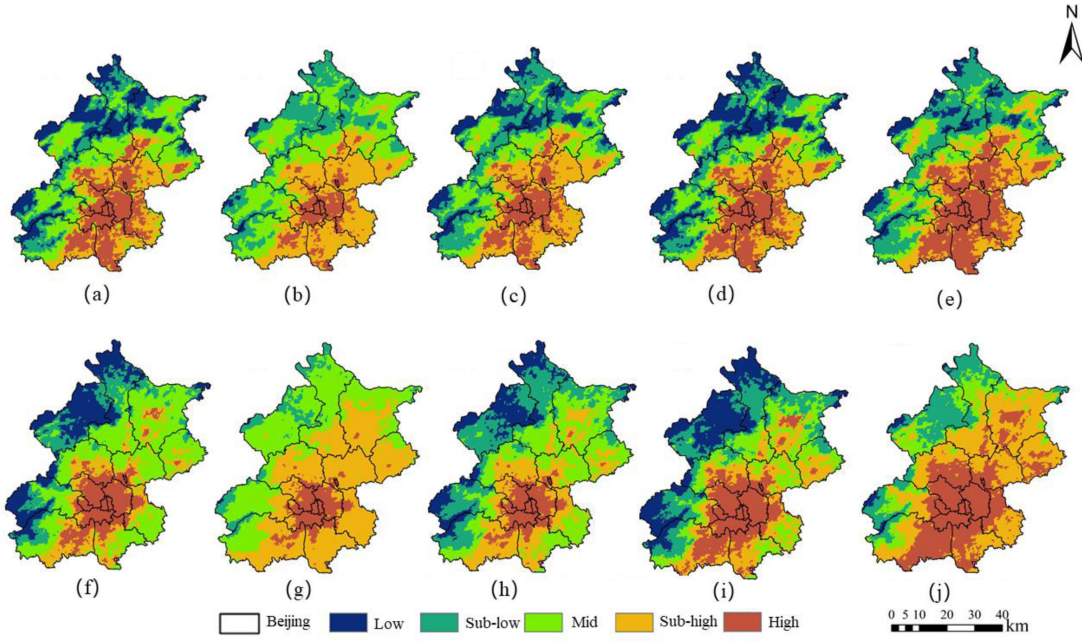


Fig. 2. Spatial distribution of LST areas in Beijing based on day and night LSTs, according to different classification methods. (a) and (f) Mean-standard deviation method. (b) and (g) Equal interval method. (c) and (h) Natural breaks method. (d) and (i) Quantile method. (e) and (j) Geometric interval method.

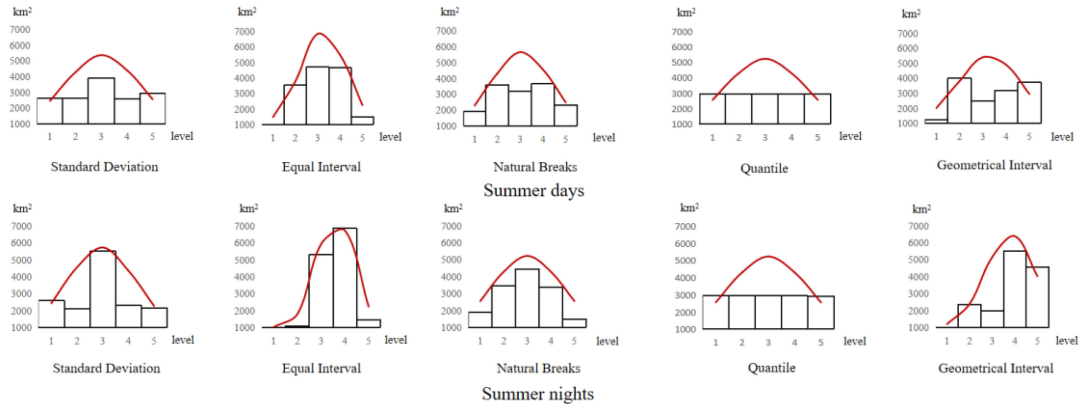


Fig. 3. Distribution of LST areas in Beijing in summer during days and nights based on five classification methods.

urban area, respectively. The nighttime UHI patch area as calculated using the equal interval and geometric interval methods exceeded 50% of the Beijing urban area. The quantile method produced the same day and night distributions for all temperature grades.

B. Reliability of Each Method Classifying UHI Areas

We used five classification methods to classify MODIS LST data covering 12 periods in summer and compared the classification results with the average LST in summer to evaluate the reliability of the different classification methods in terms of identifying UHI patches (see Fig. 4). Areas with high-temperatures and subhigh-temperatures relative to the average LST in summer were defined as UHI patches. Judging from the classification results while considering the average LST in summer, the summer

daytime UHI patch area estimated by the mean-standard deviation method for Beijing in 2020 was the smallest, accounting for 33.39% of the urban area of Beijing, and the urban area obtained by the geometric interval method produced the largest estimated area (42.28%). The areas classified by the other three classification methods were similar. Furthermore, the UHI patch area at night in summer was similar to that in the day, with the proportional UHI patch area (of the total Beijing area) obtained using the mean-standard deviation method the smallest. The UHI patch area obtained using the geometric interval classification was the largest (61.52%), whereas the area obtained using the natural breaks method was closer to that obtained using the mean-standard deviation method. Because MODIS data are inevitably affected by clouds over an eight-days, this article determined that the pixels classified as having high-temperatures and subhigh temperatures in 10 or more periods out of 12 periods would represent UHI patches. We then further evaluated whether

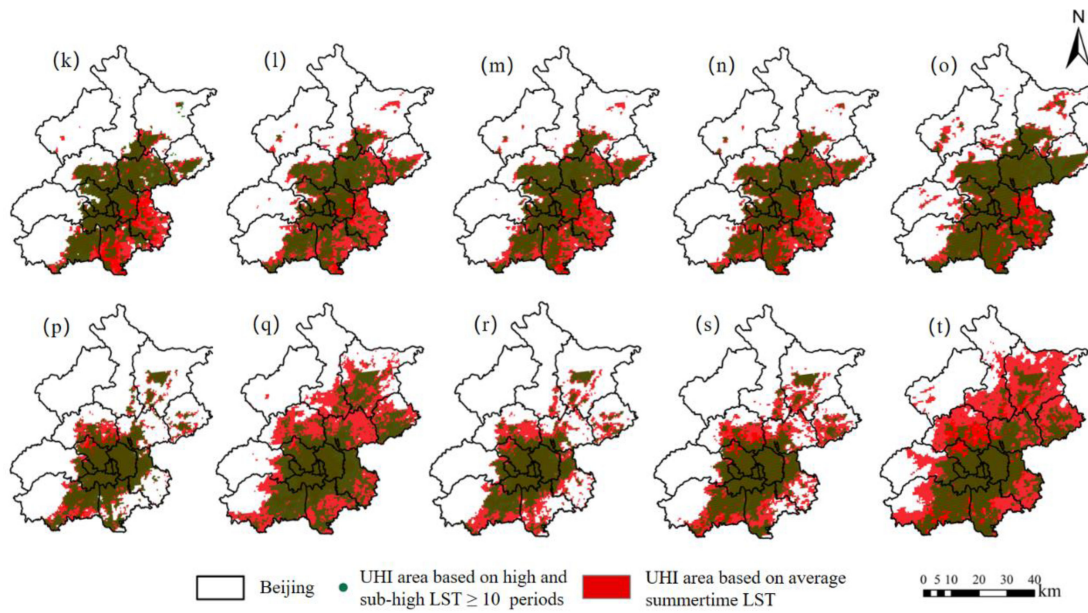


Fig. 4. Robustness analysis of LST areas classification by different classification methods.

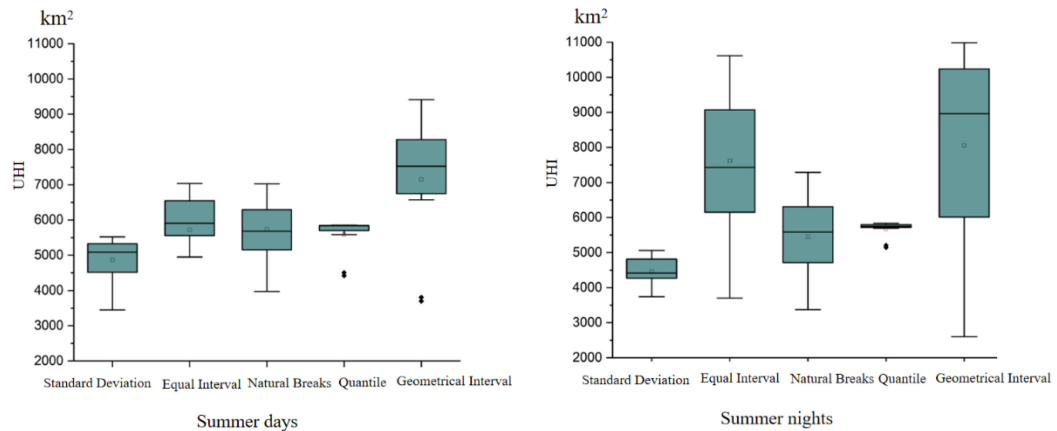


Fig. 5. Box plots of the UHI area during summer days and nights in Beijing in 2020.

the selected data overlapped with UHI patches identified based on the average summer surface temperature. During the day in Summer, the pixels selected by each classification method based on 12-period MODIS LST data accounted for the following proportion of the UHI patch area identified using the average summertime LST (ordered from high to low): geometric interval method, 75.84%; quantile method, 64.70%; natural breaks method, 62.60%; mean-standard deviation method, 54.78%; and equal interval method, 42.20%. For summer nights, the methods were ranked from high to low was as follows: natural breaks method (57.94%) > equal interval method (56.21%) > quantile method (55.67%) > mean-standard deviation method (52.47%) > geometric interval method (37.78%). The mean-standard deviation and natural breaks methods produced the most stable proportions for day- and nighttime, with the error rate not exceeding 4.66% (mean-standard deviation method: 2.31%; natural breaks method: 4.66%). Therefore, the mean-standard deviation and

natural breaks methods were less disturbed by data quality (e.g., clouds, etc.) and were more robust in terms of the classification of land surface heat levels.

C. Robustness of Estimating UHI Area and UHI Intensity Using Different Standard Classification Methods

We compared the robustness of estimating the UHI patch area and intensity using 12-period summertime data analyzed with. For summer days the geometric interval method produced the largest average and median UHI area (7147.25 and 7525.50 km², respectively), whereas the mean-standard deviation method produced the smallest values (4843.42 and 5085.00 km², respectively); the quantile method produced average and median UHI areas with the closest values (5587.58 and 5835.00 km², respectively). The geometric interval method provided the largest maximum-to-minimum range and variance. The quantile

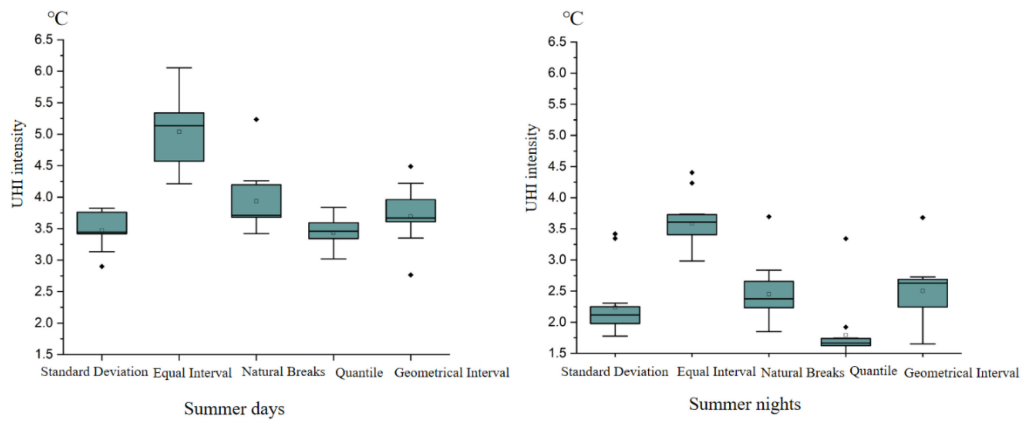


Fig. 6. Box plot of the UHI intensity during summer days and nights in Beijing in 2020.

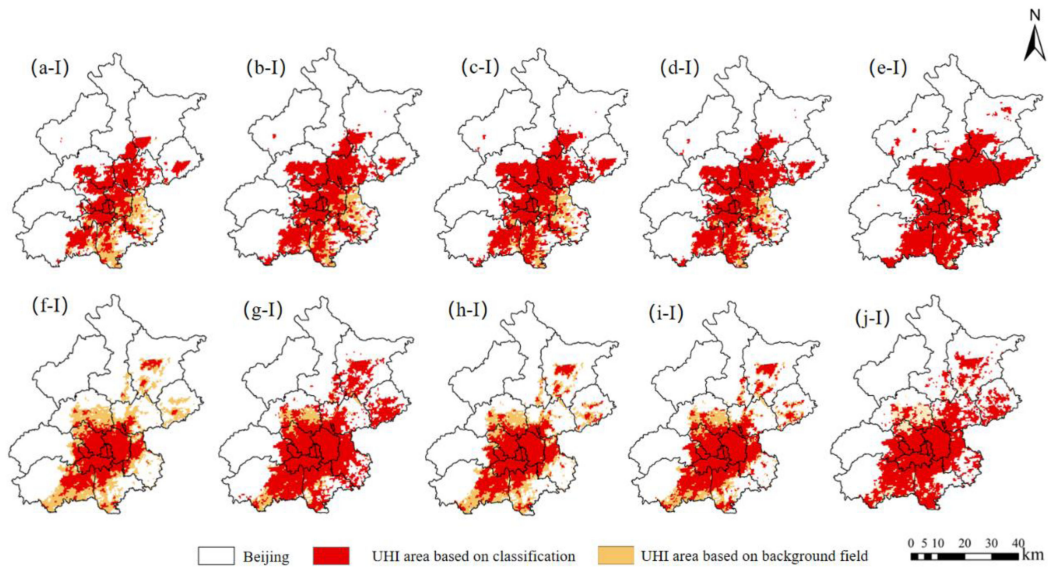


Fig. 7. Comparison of UHI area determined based on classification and the background method. (a-I) and (f-I) Mean-standard deviation method. (b-I) and (g-I) Equal interval method. (c-I) and (h-I) Natural breaks method. (d-I) and (i-I) Quantile method. (e-I) and (j-I) Geometric interval method.

TABLE I
KAPPA COEFFICIENTS FOR THE UHI AREA DETERMINED BASED ON CLASSIFICATION AND THE BACKGROUND METHOD

Time	Classification Methods				
	Standard Deviation	Equal Interval	Natural Breaks	Quantile	Geometrical Interval
Summer days	0.60	0.53	0.55	0.56	0.47
Summer nights	0.99	0.54	0.93	0.77	0.45

method produced the smallest values; however, we noticed that the quantile method also produced several outlier values. The night and day conditions in summer were similar. Thus, the results of classification by the geometric interval method based on LST grades exhibited significant volatility, whereas variability due to the mean-standard deviation and quantile methods was low (see Fig. 5). Therefore, for classifying the UHI area, the

mean-standard deviation, quantile, and natural breaks methods were the most stable and accurate.

The UHI intensity during the day in summer was higher than that at night, and the values obtained using the equal interval method were the highest (day: 5.09 °C; night: 3.86 °C), whereas the quantile method produced the lowest values (day: 3.72 °C; night 1.79 °C). During the summer daytime, the highest average

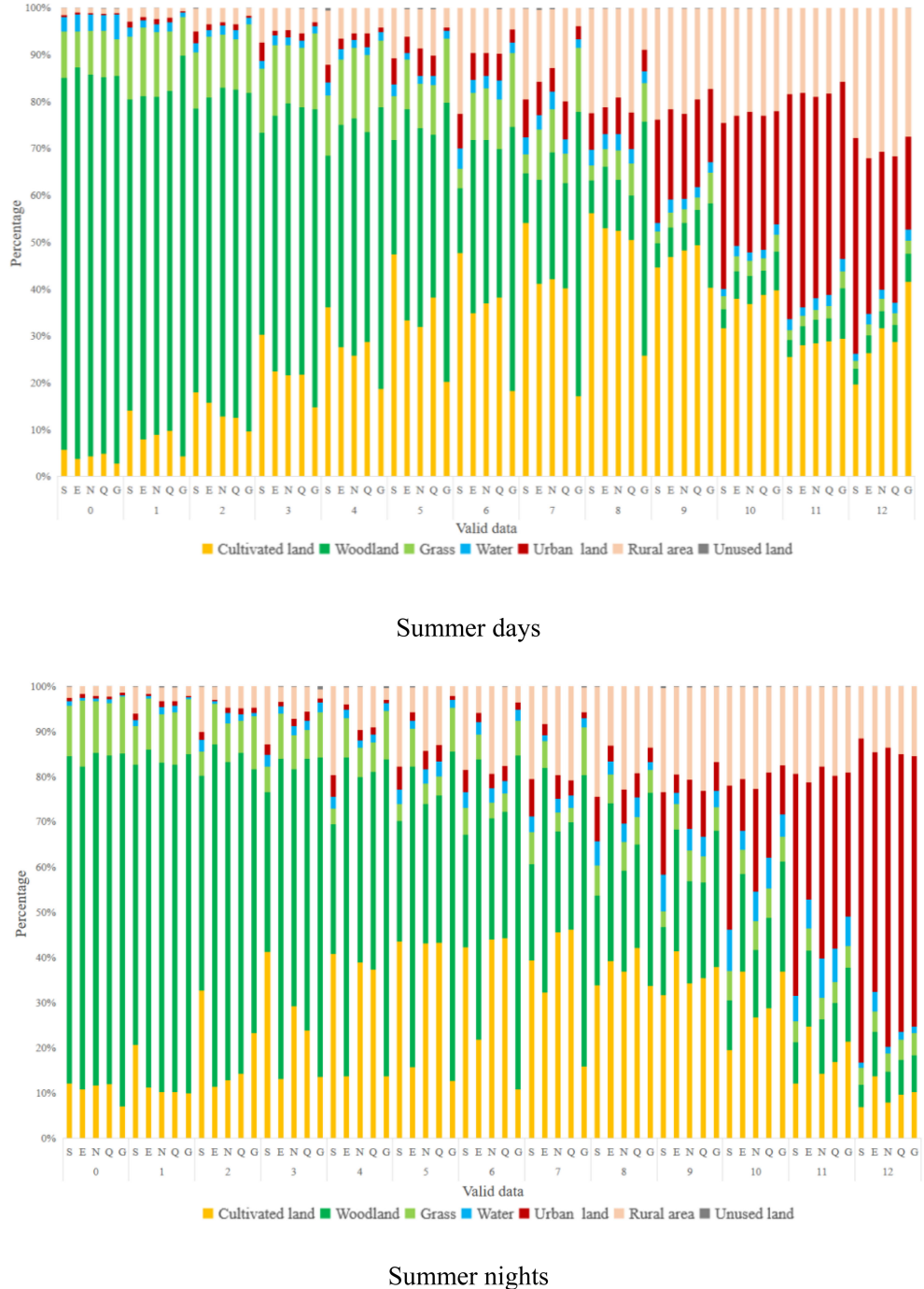


Fig. 8. Proportions of land use types for each period for which data were valid. “S,” “E,” “N,” “Q,” and “G” represent the standard deviation method, the equal interval method, the natural breaks (Jenks) method, the quantile method, the geometrical interval method, respectively.

and median UHI intensities were obtained with the equal interval method (5.09°C and 5.16°C , respectively), and the average UHI intensity estimated using the quantile method was the lowest (3.44°C) (see Fig. 6). However, the mean-standard deviation method produced the smallest median UHI intensity (3.45°C). The widest range between the maximum and minimum values and the largest variance for UHI intensity were obtained using the equal interval method, with the smallest obtained using the quantile method. For summer nights in Beijing, the highest

average and median UHI intensities were found using the equal interval method (3.52°C and 3.56°C , respectively), and the lowest values were obtained with the quantile method (1.67°C and 1.66°C , respectively); the analysis for summer days produced similar values. Although the maximum-to-minimum range of UHI intensity and the variance differed from those for summer days, the results obtained using the geometric interval method exhibited the largest fluctuations, and the results obtained using the quantile method had the smallest fluctuations. Therefore, for

UHI intensity, the quantile, the mean-standard deviation, and the natural breaks methods were the most robust.

IV. DISCUSSION

A. Classifying UHI Areas Using Different Methods

Starting from the concept of a UHI itself (that is, an urban area where the temperature is higher than those of the surrounding suburbs), calculating the UHI intensity is a widely used method in current research on UHIs [32]–[34]. This article selected cropland 5–20 km from the Beijing central city area at an altitude of 0–60 m as the rural area to determine the UHI area using five classification methods to evaluate the accuracy of the methods in identifying UHIs (see Fig. 7). We compared the kappa coefficients of the UHI patches obtained using the five classification methods and UHI patches identified using traditional methods, to determine the overlap rate. The kappa coefficients of the mean-standard deviation and natural breaks (Jenks) methods were 0.99 and 0.93, respectively, indicating that the UHI area determined using the two classification methods was highly consistent with that determined based on the background field (kappa > 0.75 indicates fairly high consistency) (see Table I).

B. Influence of Land-Use Type Composition on UHI Areas

We classified 12-period LST data from Beijing into different categories using five classification methods and analyzed the distribution of land use types in the UHI patches identified by the classification methods (see Fig. 8). By only comparing valid data over the 12 periods, regular changes in the land-use composition of UHI patches were observed. For summer days and nights, the more periods data used to define UHI patches in Beijing were valid over, the higher the ratio of urban construction land to rural residential area, with the most significant increase observed when the data were valid over 10 or more periods. Based on Section IV-B of the Results, this article determined that the data would be valid over ten or more periods to identify UHI patches.

The different land use types in UHI were analyzed using different classification methods. For daytime in summer, the ratio of urban construction land to rural residential area in the UHI patch area estimated using each method were ranked (from high to low) as follows: mean-standard deviation method > equal interval method > natural breaks method > quantile method > geometric interval method. For summer nights, the order was as follows: mean-standard deviation method > natural breaks method > quantile method > geometric interval method > equal interval method. Taken together, the classification results for summer days and nights showed that the classification of areas as UHI patches by the mean-standard deviation and natural breaks methods was reasonable, given the land use types present in these areas.

V. CONCLUSION

The article aimed to explore the robustness of UHI patch classification using different standard classification methods, in an attempt to provide a guide for the selection of an urban

surface thermal classification method using thermal infrared remote-sensing data. The article used the 12 periods of eight-day MODIS LST data captured during the summer of 2020 in Beijing, as well as the average summer LST, to classify land surface heat levels and define UHI patches. In the comparison of the robustness of the five methods, we focused on two indicators: UHI area and UHI intensity. The UHI classification methods were then evaluated from the perspective of traditional methods and actual land use. In terms of the spatial distribution and areal proportions of regions with different thermal levels, the results obtained by mean-standard deviation method and natural breaks methods more closely approximated the actual situation. In identifying likely UHI patches during the day and night in summer in Beijing, the mean-standard deviation and the natural breaks methods were more effective. The robustness of the classification methods was compared based on UHI patch area and UHI intensity. The quantile, mean-standard deviation, and natural breaks methods were more stable, whereas the mean-standard deviation and natural breaks methods displayed good reliability. From the perspective of land use, the land use composition of the UHI patches classified by the mean-standard deviation and natural breaks methods produced the highest ratio of urban construction land to residential area, which is expected in a UHI patch. By comparing the kappa coefficients, we determined that the areas identified by the mean-standard deviation and natural breaks methods as UHI patches were the closest to those identified using traditional methods. Thus, this article provides a comparison of classification methods and guidance on the basic data needed for identifying UHI patches and exploring spatiotemporal changes in UHIs.

This article has several limitations. First, because the study was to explore the effectiveness of different standard classification methods in identifying UHI patches, there was no discussion on establishing strict boundaries between urban and rural areas when calculating the UHI intensity. The middle temperature was selected as the average rural temperature, such that the estimated UHI intensity for these areas was low. Second, we only discussed how different standard classification methods identify UHIs in Beijing. In other regions, these methods may identify UHIs differently. Thus, additional work in this area should consider if there are general characteristics that can be employed to classify data for identifying UHI areas, with respect to determining the most suitable classification method.

REFERENCES

- [1] J. Yang *et al.*, “Understanding land surface temperature impact factors based on local climate zones,” *Sustain. Cities Soc.*, vol. 69, no. 3, pp. 102818–102828, Mar. 2021.
- [2] T. R. Oke *et al.*, *Urban Climates*, London, U.K.: Cambridge Univ. Press, 2017.
- [3] B. J. He *et al.*, “Potentials of meteorological characteristics and synoptic conditions to mitigate urban heat island effects,” *Urban Climate*, vol. 24, no. 6, pp. 26–33, Jun. 2018.
- [4] S. Orhun, “Effects of landscape composition and patterns on land surface temperature: Urban heat island case study for Nigde, Turkey,” *Urban Climate*, vol. 34, no. 11, pp. 1–18, Dec. 2020.
- [5] D. Zhou *et al.*, “Satellite remote sensing of surface urban heat islands: Progress, challenges, and perspectives,” *Remote Sens.*, vol. 11, no. 1, pp. 1–6, Jan. 2018.

- [6] J. Yang *et al.*, "Optimizing local climate zones to mitigate urban heat island effect in human settlements," *J. Cleaner Prod.*, vol. 275, no. 12, pp. 123767–112375, Dec. 2020.
- [7] J. Yang *et al.*, "Contribution of urban ventilation to the thermal environment and urban energy demand: Different climate background perspectives," *Sci. Total Environ.*, vol. 795, no. 34, pp. 1–12, Jul. 2021.
- [8] D. Q. Sun *et al.*, "Examining spatio-temporal characteristics of urban heat islands and factors driving them in Hangzhou, China," *IEEE J. Sel. Topics Appl. Earth Observ. Remote Sens.*, vol. 14, no. 5, pp. 8316–8325, May 2021.
- [9] A. D. Guo *et al.*, "Impact of urban morphology and landscape characteristics on spatiotemporal heterogeneity of land surface temperature," *Sustain. Cities Soc.*, vol. 63, no. 1, pp. 102443–102465, Jan. 2020.
- [10] J. Yang *et al.*, "Simulation of landscape spatial layout evolution in rural-urban fringe areas: A case study of Ganjingzi district," *GISci. Remote Sens.*, vol. 56, no. 3, pp. 388–405, Apr. 2019.
- [11] H. L. You *et al.*, "Spatial evolution of population change in Northeast China during 1992–2018," *Sci. Total Environ.*, vol. 779, no. 2, pp. 146023–146031, 2021.
- [12] Y. Lu *et al.*, "Investigating the spatiotemporal non-stationary relationships between urban spatial form and land surface temperature: A case study of Wuhan, China," *Sustain. Cities Soc.*, vol. 72, no. 6, pp. 103070–103082, Jun. 2021.
- [13] L. Hou *et al.*, "Spatiotemporal patterns and drivers of summer heat island in Beijing-Tianjin-Hebei urban agglomeration, China," *IEEE J. Sel. Topics Appl. Earth Observ. Remote Sens.*, vol. 14, no. 1, pp. 7516–7527, Jan. 2021.
- [14] B. J. He, L. Ding, and D. Prasad, "Wind-sensitive urban planning and design: Precinct ventilation performance and its potential for local warming mitigation in an open midrise gridiron precinct," *J. Building Eng.*, vol. 29, no. 5, pp. 101145–101164, May 2020.
- [15] X. Liu *et al.*, "Estimating multi-temporal anthropogenic heat flux based on the top-down method and temporal downscaling methods in Beijing, China," *Resour., Conserv. Recycling*, vol. 172, no. 6, pp. 105682–105695, Jun. 2021.
- [16] Z. Qiao *et al.*, "Spatio-temporal pattern and evolution of the urban thermal landscape in metropolitan Beijing between 2003 and 2017," (in Chinese), *Acta Geographica Sinica*, vol. 74, no. 3, pp. 475–489, Mar. 2019.
- [17] T. Peng *et al.*, "Assessing spatiotemporal characteristics of urban heat islands from the perspective of an urban expansion and green infrastructure," *Sustain. Cities Soc.*, vol. 74, no. 1, pp. 1–14, Aug. 2021.
- [18] Y. Fan *et al.*, "Analysis of Guangzhou's urban expansion and its urban heat island effect," (in Chinese), *Remote Sen. Inf.*, vol. 29, no. 1, pp. 23–29, Feb. 2014.
- [19] R. Lin, X. Qi, and S. Ye, "Spatial-temporal characteristics of urban heat islands and driving mechanisms in a Coastal Valley-basin city: A case study of Fuzhou city," (in Chinese), *Acta Ecologica Sinica*, vol. 37, no. 1, pp. 294–304, Jan. 2017.
- [20] J. Pan, "Area delineation and spatial-temporal dynamics of urban heat island in Lanzhou city, China using remote sensing imagery," (in Chinese), *J. Indian Soc. Remote Sens.*, vol. 44, no. 1, pp. 111–127, Feb. 2016.
- [21] J. Yang *et al.*, "Investigating the diversity of land surface temperature characteristics in different scale cities based on local climate zones," *Urban Climate*, vol. 34, no. 12, pp. 100700–100712, Dec. 2020.
- [22] R. M. Smith, "Comparing traditional methods for selecting class intervals on choropleth maps, land surface temperature impact factors," *Professional Geographer*, vol. 38, no. 1, pp. 1–6, Mar. 1986.
- [23] J. Liu *et al.*, "The spatiotemporal pattern and new characteristics of land use change in China from 2010 to 2015," *Acta Geographica Sinica*, vol. 73, no. 5, pp. 789–802, Apr. 2018.
- [24] Z. Qiao *et al.*, "Determining the boundary and probability of surface urban heat island footprint based on a logistic model," *Remote Sens.*, vol. 11, no. 6, pp. 1–12, Jun. 2019.
- [25] Z. Qiao *et al.*, "Prediction and analysis of urban thermal environment risk and its spatiotemporal pattern," (in Chinese), *Acta Ecologica Sinica*, vol. 39, no. 2, pp. 649–659, Oct. 2019.
- [26] G. Liu, *Principles of Statistics*, (in Chinese), 3rd ed., Shanghai, China: East China Univ. Sci. Technol. Press, 2016.
- [27] H. Yin *et al.*, *Urban Planning-Experiment-Textbook-Regional Planning*, (in Chinese), Nanjing China: Southeast Univ. Press, 2016.
- [28] N. Mu *et al.*, *ArcGIS Engine Geographic Information System Development Tutorial*, (in Chinese), Nanjing, China: Surv. Mapping Press, 2015.
- [29] M. J. Smith *et al.*, *Geospatial Analysis*. 6th ed., England: The Winchelsea Press, 2018.
- [30] Z. Qiao *et al.*, "The impact of urban renewal on land surface temperature changes: A case study in the main city of Guangzhou, China," *Remote Sens.*, vol. 794, no. 12, pp. 566–576, Mar. 2020.
- [31] Z. Qiao *et al.*, "Scale effects of the relationships between 3D building morphology and urban heat island: A case study of provincial capital cities of mainland China," *Complexity*, vol. 2020, no. 11, pp. 1–12, Nov. 2020.
- [32] H. Shi *et al.*, "Urban heat island and its regional impacts using remotely sensed thermal Data-A review of recent developments and methodology," *Land*, vol. 10, no. 8, pp. 1–30, Aug. 2021.
- [33] R. D. Feng *et al.*, "Urban ecological land and natural-anthropogenic environment interactively drive surface urban heat island: An urban agglomeration-level study in China," *Environ. Int.*, vol. 157, no. 12, pp. 106857–106869, Dec. 2021.
- [34] K. G. Li *et al.*, "Comparative analysis of variations and patterns between surface urban heat island intensity and frequency across 305 Chinese cities," *Remote Sens.*, vol. 13, no. 17, pp. 3505–3523, Sep. 2021.

Yingshuang Lu is a postgraduate student with the School of Environmental Science and Engineering, Tianjin University, Tianjin, China, majoring in resources and environment.

Tong He is working toward the Master degree in resources and environment with Tianjin University, Tianjin, China.

Xinliang Xu received the Ph.D. degree in cartography and geographic information systems from the Chinese Academy of Sciences, Beijing, China.

He is a Professor with the Institute of Geographic Sciences and Natural Resources Research, Chinese Academy of Sciences, Beijing, China. His research interests include resource and environmental information system research and development, remote sensing monitoring of land use/cover change and monitoring and evaluation of its environmental effects and ecosystem service functions.

Zhi Qiao received the Ph.D. degree in environmental science from Beijing Normal University, Beijing, China.

He is currently an Associate Professor with the School of Environmental Science and Engineering, Tianjin University, Tianjin, China. His main research interests include application of GIS and remote sensing technology in environmental science and ecology, land use change, and urban thermal environment.